Available online at www.sciencedirect.com
ScienceDirect
Image and Vision Computing 25 (2007) 1282–1290
www.elsevier.com/locate/imavis

Contour detection based on contextual influences

Qiling Tang [a], Nong Sang [a,*], Tianxu Zhang [b]

[a] Institute for Pattern Recognition and Artificial Intelligence, Huazhong University of Science and Technology, Wuhan 430074, PR China
[b] Key Laboratory of Ministry of Education for Image Processing and Intelligent Control, Wuhan 430074, PR China

Received 28 March 2005; received in revised form 20 April 2006; accepted 9 August 2006

Abstract

A contour detection model, inspired by the behavior of the primary visual cortex, is presented. The response of a central stimulus in the receptive field is affected by the presence of surrounding stimuli – for some stimulus conditions, the response is suppressed and for other conditions the response is enhanced. The visual mechanisms of contextual influences are utilized to extract "coherent" configurations. This is mainly due to the following two reasons: (1) on the one hand, a smooth contour can yield collinear excitation, which highlights smooth contours from irregularly textured surround; (2) on the other hand, similar orientation textures receive iso-orientation surround suppression and region boundary is subjected to the less inhibition, which makes boundary more salient for perceptual pop-out. Accordingly, smooth contours progressively stand out from their surround and at the same time textures are gradually suppressed by their surround through dynamic fine-tuning of contextual information. The proposed method which distinguishes between contours and texture edges is more effective for contour-based object recognition tasks. Initial experiments show that the model can be successfully applied to contour detection. Especially, when object contours are lumped together with unwantedly cluttered surround, the advantage of our approach is more prominent. This study provides a biological scheme for contour detection in computer vision.

Keywords: Contour detection; Contextual influences; Visual mechanisms; Suppression; Enhancement

1. Introduction

Edge detection is a foundation of image segmentation and feature extraction and plays an important role in image analysis and understanding. Consequently, it is one of the most intensively studied subproblems in computer vision. Many edge detection algorithms have been reported, whereas most of the edge detectors do not distinguish between object contours and edges originating from textured regions [1–5], so that their results contain lots of unwanted edges which make part of texture. However, so far as human visual perception is concerned, smooth contours with coherent spatial configurations and texture boundaries where there is a change in orientation have the higher saliencies and can be more easily detected. The visual mechanisms provide a biological strategy for contour detection.

Grigorescu et al. [6] used the method of non-classical receptive field (non-CRF) inhibition to effectively suppress surrounding textures and admirably preserve isolated contours. They regarded isolated lines and edges as non-texture features, which are not affected by the inhibition, while groups of lines and edges viewed as texture features are suppressed. But there exist two major defects in their work: (1) owing to taking only surround inhibition effect into account, contours will also be inhibited as textures when contours are embedded in textured surround; and (2) their model lacks of a dynamic feedback mechanism, thus the ability to utilize contextual interactions is limited. For smooth contours, in addition to the surround inhibition, what is more, "coherent" configurations produce collinear excitation by contextual interactions, which makes contours relatively more salient and pop out from the background.

* Corresponding author. Tel.: +86 27 87541761; Fax: +86 27 87543594.
E-mail addresses: tqlinn@sohu.com (Q. Tang), nsang@hust.edu.cn (N. Sang).

0262-8856/$ - see front matter © 2006 Elsevier B.V. All rights reserved.
doi:10.1016/j.imavis.2006.08.007

Stimuli outside classical receptive fields exert a significant influence over the activities of neurons in the primary visual cortex. Parallel physiological and anatomical studies of striate cortex in cat and monkey revealed similar lateral interactions mediated by short- and long-range horizontal connections showing collinear excitation and iso-orientation surround inhibition [7–12]. Levitt and Lund [13] demonstrated that the responses to a stimulus placed within a V1 neuron's receptive field can be either increased or decreased by adding a stimulus in the region surrounding the receptive field. Knierim and van Essen [14] observed experimentally that the response to stimulus in the CRF is suppressed significantly by similarly oriented stimuli in the surround – iso-orientation suppression. The suppression is reduced when the orientations of the surround stimuli are random or different from the stimulus in the RF. However, if the surround stimuli are aligned with the optimal stimulus inside the RF to form a smooth contour, then suppression becomes facilitation [15,16]. Whether the response to stimuli presented within the receptive field can be enhanced or suppressed by other stimuli falling outside the receptive field depends on the relative orientation of pattern elements inside and outside the receptive field [17]. Bonneh and Sagi [8] found that detectability depends on stimulus geometry and is constrained by collinearity and proximity spatial relationships, and therefore a 'coherent' configuration (e.g. smooth contour) is more easily detected than a 'non-coherent' one (e.g. jagged contour).

Li's research [16,18] manifested further that the contextual influence can indeed selectively enhance neural responses to segments of smooth contours against a noisy background. They considered that pre-attentive visual mechanisms in V1 locate the region boundaries by locating where homogeneities or translation invariance in inputs break down, and highlight such locations by higher neural responses. Strengthening neural responses to these important image locations make the neural activities near boundaries higher than elsewhere. [19] supposed that the neurons in the prime visual cortex perform contour detection in a functional network fashion.

The mechanisms of visual perception provide a biological method for salient contour detection. According to the characteristics that local elements on the smooth contour have coherent spatial configurations, we detect contours through the interactions of the contextual information, strengthening coherent configurations while weakening surrounding textures.

The paper is organized as follows. In Section 2 we use Gabor energy filters to model the function of complex cells and introduce the mechanisms of inhibition and enhancement. In Section 3, some practical aspects in the application of the method are discussed, and then we test the performance of this algorithm through various synthetic and natural images, and compare with Gabor energy edge detector and the contour detection operators proposed by Grigorescu et al. Finally, we draw conclusions and present future work in Section 4.

2. Algorithm implementation

2.1. Spatial filters

Most simple cells in the primary visual cortex are selective for orientation of patterns falling within a restricted region of visual space [20–22]. These cells have their own preferred orientations within the range of θ to $\pi/2$. These simple cells behave in approximately linear fashion, and thus they can be regarded as linear spatial filters [23]. Psychophysical and physiological evidences suggest that the visual input is first decomposed by local analyzers or channels tuned to specific properties such as orientation, spatial frequency and direction of motion [8]. As linear filters, 2D Gabor functions with selected frequency and orientation can effectively model the receptive field profiles of simple cells in mammalian visual cortex [24–26], which realizes mathematical formulation of the receptive field.

A Gabor function is a Gaussian modulated by a complex sinusoid, as the following equation illustrates:

$$h(x,y) = g(x',y')\exp(j2\pi Fx') \tag{1}$$

where $(x',y') = (x\cos\theta + y\sin\theta, -x\sin\theta + y\cos\theta)$, θ denotes the orientation of the filter. Any desired orientation can be achieved via a rigid rotation in the x–y plane. F denotes the spatial center frequency, which determines the position of center of a bandpass filter in the frequency domain. $g(x,y)$ is the following 2-D Gaussian:

$$g(x,y) = \frac{1}{2\pi\sigma_x\sigma_y}\exp\left\{-\frac{1}{2}\left[\left(\frac{x}{\sigma_x}\right)^2 + \left(\frac{y}{\sigma_y}\right)^2\right]\right\} \tag{2}$$

where σ_x and σ_y denote the horizontal and vertical spatial extent of the filter, and they are utilized to determine the size of the RF. The values of σ_x and σ_y are related to the half-peak magnitude frequency bandwidth and orientation bandwidth of the filter, and are given by [27]

$$\sigma_x = \sqrt{\frac{\ln 2}{2}}\frac{1}{\pi F}\frac{2^{B_F}+1}{2^{B_F}-1} \tag{3}$$

$$\sigma_y = \sqrt{\frac{\ln 2}{2}}\frac{1}{\pi F}\frac{1}{\tan(B_\theta/2)} \tag{4}$$

where the frequency bandwidth in octaves, B_F, reflects the localization capability of the filter in the spatial and frequency domains, and the orientation bandwidth in radians, B_θ, reflects the localization capability of the filter for orientations.

Morrone and Burr [28] showed that the maxima of local energy occur at points where the phases of the Fourier components are maximally similar. They suggested that feature detection in human visual system proceeds by first computing the local energy at every point in the retinal image and then searching for the local maxima. In the local energy model, a given image is filtered with a set of filters that have identical amplitude spectra but orthogonal phase spectra [29]. The Gabor function is chosen to implement the local energy model because it is highly directional

and models well the receptive field profiles of simple cells in the primate visual cortex [29,30]. Using the response modulus of odd–even pairs of Gabor filters, i.e. the square root of summing the squared responses of the filters, can capture the typically fundamental characteristics of complex cells [31,32]. The operator can correctly characterize edges and lines presented in natural images.

The real component and the imaginary component of a Gabor function are symmetric and antisymmetric respectively; their definitions are as follows:

$$h_e(x,y) = g(x',y')\cos(2\pi Fx') \tag{5}$$

$$h_o(x,y) = g(x',y')\sin(2\pi Fx') \tag{6}$$

The response modulus of orthogonal pairs of Gabor filters is called Gabor energy, and can be expressed as follows:

$$E(x,y) = \sqrt{r_e^2(x,y) + r_o^2(x,y)} \tag{7}$$

where $r_e(x,y) = h_e(x,y)*f(x,y)$, $r_o(x,y) = h_o(x,y)*f(x,y)$, $*$ denotes convolution, f is an image.

2.2. Iso-orientation suppression

The response of neuron to a stimulus in the RF is suppressed by the iso-orientation surrounding stimuli outside the RF. Fig. 1 illustrates the iso-orientation suppression effect by an example used in psychophysical experiment. In this case, line elements with similar orientations inhibit each other, which causes the middle line segments with different orientations from the background to pop out perceptually for pre-attentive vision. The physiological and psychophysical findings have shown that inhibitory intensities decrease with increasing distance from the center of the RF. We adopt the inhibitory weighting model established by Grigorescu et al. [6]. For a given point in the image, the inhibition term is computed in a ring-formed area surrounding the RF centered at the concerned point, see Fig. 2. The weighting function $w_\sigma(x,y)$ is normalized as follows:

$$w_\sigma(x,y) = \frac{1}{\|H(DoG_\sigma)\|_1} H(DoG_\sigma(x,y)) \tag{8}$$

$$H(z) = \begin{cases} 0, & z < 0 \\ z, & \text{else} \end{cases} \tag{9}$$

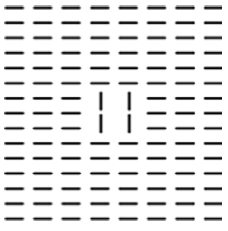

Fig. 1. An example used by psychophysical experiment to illustrate iso-orientation suppression.

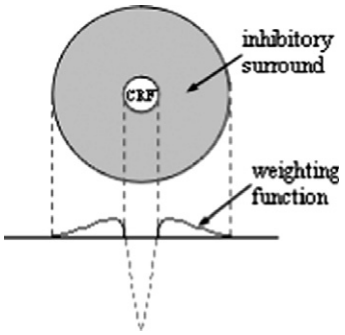

Fig. 2. Non-CRF inhibition is defined by the weighting function.

where $\|\cdot\|_1$ denotes the L_1 norm, the function $H(z)$ ensures to generate inhibitory action only in the non-CRF, and $DoG_\sigma(x,y)$ is the following difference of Gaussian functions:

$$DoG_\sigma(x,y) = \frac{1}{\sqrt{2\pi}4\sigma} e^{-\frac{x^2+y^2}{2(4\sigma)^2}} - \frac{1}{\sqrt{2\pi}\sigma} e^{-\frac{x^2+y^2}{2\sigma^2}} \tag{10}$$

The inhibitory region is specified by $x^2 + y^2 = 4\sigma^2$ (see [6] for details); here $\sigma = \sigma_x$.

The research of Knierim et al. [14] have shown that suppression depends on the relative orientations of the centre and surround stimuli: suppression is strongest when the surround stimuli are of the same orientation as the centre stimulus, is weaker when the surround stimuli have random orientations and is weakest when the surround stimuli are oriented orthogonally to the centre stimulus [14,16]. In order to describe the degree of suppression varying according to the orientation similarity, an orientation contrast-based weighting function is given by,

$$k(\theta_\Delta) = e^{-8(\theta_\Delta/\pi)^{1.5}} \tag{11}$$

where these coefficients are chosen empirically. To explain this empirical finding, we investigated the sensitivity of various tests. The sensitivity analysis has shown that the choice is extensively adaptable and this may provide a plausible explanation for the influence of orientation contrast. θ_Δ denotes orientation contrast between the centre and surround stimuli; its definition is as follows:

$$\theta_\Delta = \min(|\theta - \theta'|, \pi - |\theta - \theta'|) \tag{12}$$

Thus, the surround inhibition from which the neuron with the preferred orientation θ suffers is computed in the following way:

$$I'_\theta(x,y) = \sum_{\theta'} k(\theta_\Delta) i'_{\theta'}(x,y) \quad \theta,\theta' \in \left\{0, \ \frac{\pi}{N}, \ \ldots, \ \frac{(N-1)\pi}{N}\right\} \tag{13}$$

where $i'_{\theta'}(x,y)$ represents the inhibition term coming from orientation θ' and can be computed as follows:

$$i'_{\theta'}(x,y) = w_\sigma(x,y) * R'_{\theta'}(x,y) \tag{14}$$

where $R^t_{\theta'}(x,y)$ denotes the image's response at the orientation θ', and superscript t is the number of iterations for the convenience of future illustration.

2.3. Collinear enhancement

Several studies have reported that enhancement depends on the precise spatial configuration (i.e., collinearity) of the surround [8,12,15]. "Coherent" configurations are more likely to attract visual attention. Fig. 3. is used to explain the collinear enhancement effect. In this example, "coherent" configurations consisting of seven line segments, running from top left to bottom right, are embedded in a background of randomly oriented distractors. As it is clear from this figure, "coherent" configurations are relatively more salient and these elements can be easily detected. Fig. 4 illustrates the contextual interactions when the center has coherent spatial configurations with its neighbors. At each location i there is a hypercolumn composed of N neurons. Each neuron with the RF center i and preferred orientation $\theta = n\pi/N$ for $n = 0, 1, \cdots, N-1$ interacts with neighboring those which have different RF centers (see [16] for details). The response of a central stimulus is affected by neighboring stimuli, when they are aligned to form a collinear configuration (as the bold lines shown in Fig. 4), the center receives collinear excitation from its neighbors, thus allowing them to pop out perceptually.

Furthermore, the enhancement depends only on the immediately adjacent surround, that is, the enhancement had no effect as the surround width is increased beyond this adjacent region, whereas the suppression relied on a much wider surround region [20]. As a result, a ring-formed area is used for long-range inhibitory interactions and an eight-neighborhood for short-range excitatory processes. With respect to the "coherent" configurations, we consider the following two facts,

(I) The orientations of the center and the surround are similar, that is, the smaller the orientation contrast between them, the stronger the enhancement is. A Gaussian weighting function is used to assign a weight to the orientation contrast.
(II) The center and the surround should be co-aligned, that is, the connecting line between the center and the surround should not deviate from the preferred orientation of the center excessively. Here, the maximum of deviation angle is set to $\pi/4$.

The neuron with the preferred orientation θ obtains the enhancement through contextual interactions as follows,

$$S^t_\theta(x,y) = \sum_{(x',y')\in V} \sum_{\theta'} w(\theta_\Delta) R^t_{\theta'}(x',y') \tag{15}$$

where $w(\theta_\Delta)$ is defined in (10). V denotes the excitatory regions of a neuron with a given orientation, consisting of only some of its nearest-neighbors whose deviation angle is less than $\pi/4$.

2.4. Model description

Now we model the visual mechanisms of contour detection based on contextual interactions through the following dynamical equation,

$$R^{t+1}_\theta(x,y) = \left[R^t_\theta(x,y) + \eta(t)\left(w_s S^t_\theta(x,y) - w_i I^t_\theta(x,y)\right)\right]^+ \tag{16}$$

$$\eta(t) = \mathrm{e}^{-0.02(t-1)} \tag{17}$$

where $[s]^+ = \max(s,0)$. The half-wave rectification operation ensures that the activity of cortical cell is positive response. w_s,w_i control the strength of enhancement and inhibition, respectively. In order to avoid time consuming iterative computation, an attenuation factor $\eta(t)$ is used. The choice of $\eta(t)$ is empirical and base on the observations that (1) the process would converge to some final configuration in an acceptable time, and (2) the process should experience enough contextual interactions. To terminate the iteration, we can define, in advance, either the maximum number of iterations or a lower bound of the change of $R^t_\theta(x,y)$ in successive steps. The Gabor energy $E(x,y)$ at orientation θ is taken as the initial value of $R^t_\theta(x,y)$. Note that for every iteration both the enhancement term $S^t_\theta(x,y)$ and the inhibition term $I^t_\theta(x,y)$ are updated according to the variation of $R^t_\theta(x,y)$, and $R^t_\theta(x,y)$ is normalized into [0,1] in order to eliminate amplitude differences.

Finally, we define a contour operator $R_C(x,y)$ with values of the maximum response of $R^t_\theta(x,y)$ over all orientations, as the iteration terminate.

$$R_C(x,y) = \max\left\{R^T_\theta(x,y) | \theta = n\pi/N, n = 1,2,\ldots N\right\} \tag{18}$$

where T is the maximum number of iterations.

Fig. 3. An example of collinear enhancement.

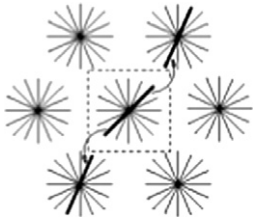

Fig. 4. Schematic diagram of contextual interactions (adapted from [16]).

3. Experiments

3.1. Parameters of the model

For Gabor filters, we choose 12 different orientations of equal intervals and five center frequencies in cycles per pixel, $F \in \{0.1000, 0.1500, 0.2250, 0.3375, 0.5063\}$. The scale factor between two successive spatial frequencies is 1.5. Usually, all filters have the same frequency bandwidth and orientation bandwidth, here frequency bandwidth B_F and orientation bandwidth B_θ are chosen to be 1.2 octaves and $\pi/6$, respectively. The values σ_x and σ_y can be obtained from Eqs. (3) and (4), respectively. The parameter w_s, w_i controlling the strength of enhancement and inhibition are set to 0.5 and 3.0, respectively, and a small variation in the parameter values would not bring salient influence to the results. The values of w_s and w_i can be adjusted according to a specific application. Finally, we choose the best results from detected contours with the above five center frequencies according to the performance measures. The selection of the parameters is used for all our experiments.

3.2. Surround inhibition process

Fig. 5 illustrates the iso-orientation inhibition process by a synthetic texture. Textons with similar orientations inhibit each other, which leads to decreasing responses in areas of uniform texture, hence highlight texture boundary locations where there is a change in orientation. It is clear that inhibition plays an important role in the segmentation of textures. The inhibition process can be implemented through shielding enhancement term from Eq. (16).

3.3. Contextual enhancement effect

Fig. 6 illustrates the effect of the enhancement. Though the curve and the line are embedded in the cluttered background, neither is flooded by the surround and appear still very distinct. This is due to the effect of the contextual enhancement, making them more salient than the background. From orientation maps, we can see that the orientations of the pixels in the curve and the straight line are coherent but those in the background are irregular. Hence, the elements with a coherent spatial structure receive collinear excitation from their neighbors, popping out from the background. Enhancement behavior is important in contour integration. The enhancement effect can be implemented through shielding inhibition term from Eq. (16).

3.4. Contour detection via inhibition and enhancement mechanisms

A circle embedded in noisy background is used to elucidate the process of the enhancement and inhibition in contour detection, as shown in Fig. 7. It is obvious that the noisy background is gradually weakened while coherent spatial configurations (smooth contours) progressively pop-out from the background with the temporal evolution of this process. The results show that the model can well detect the smooth contours despite heavy noise superimposed on the objects.

Finally, we apply the visual mechanisms to detect contours of natural images and compare the proposal with the contour detection operators by Grigorescu et al. A non-maxima suppression procedure is performed and binary contour maps are obtained using hysteresis thresholding [1]. We determine the hysteresis thresholds adaptively through examination of the histogram of gradient magnitudes [33]. For the convenience of the performance evaluation, an associated hand-drawn desired contours illustrating heavy concentration of object-related shape information is given for each image.

From the above experimental results as shown in Fig. 8, we can observe that the contours of detected objects are

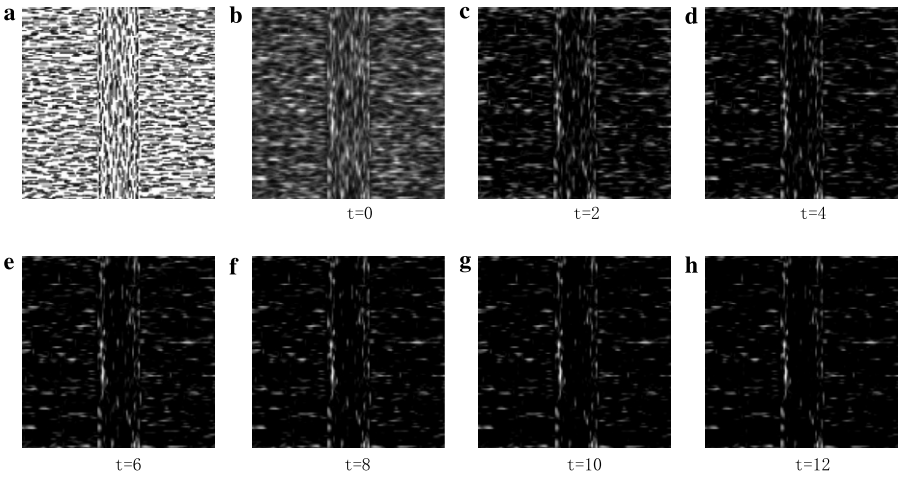

Fig. 5. Iso-orientation inhibition process. (a) Input texture image. (b) Gabor energy. (c–h) Saliency maps in iteration process. t denotes the number of iterations. The intensities rang from 0 to 255.

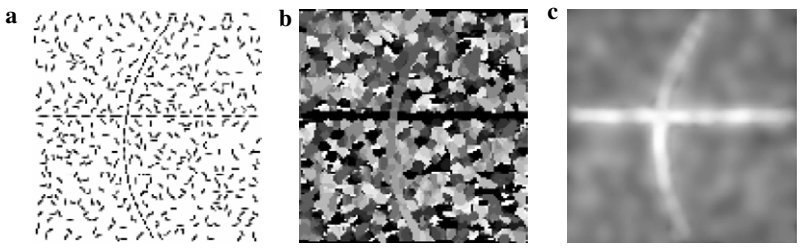

Fig. 6. Contextual enhancement effect. (a) Input image. (b) Orientation maps. Each orientation is mapped to a gray level, so 12 gray levels are used. It is the orientation at which the response reaches the maximum. (c) Saliency map resulting from contextual enhancement after 12 iterations. The intensities rang from 0 to 255.

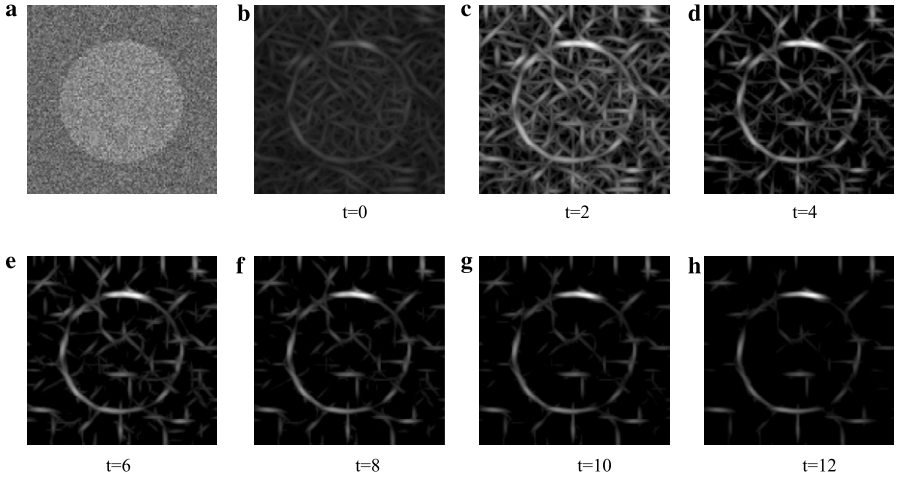

Fig. 7. Model enhancement and inhibition mechanisms to contour detection. (a) A circle embedded in a Gaussian noise background. (b–h) Saliency maps resulting from iteration process. t denotes the number of iterations. The intensities rang from 0 to 255. The spatial frequency filters $F = 0.1500$.

embedded in a cluttered or textured surround. If contours are not told from textures, it is inevitable that detected results would contain plenty of spurious structures, such as the contours obtained with Gabor energy operator. On the other hand, If mere inhibition behavior is taken into consideration, the contours will be suppressed too despite of eliminating lots of surrounding textures, as can be seen from the results obtained with anisotropic inhibition and isotropic inhibition operators. According to the configurational feature of smooth contours, we introduce enhancement behavior besides inhibition behavior, and furthermore adopt a dynamic process to imitate the visual mechanisms of contour detection. Through contextual interactions, contours with coherent spatial configurations are retained, while plenty of unwanted textures are eliminated.

3.5. Performance measures

We adopt a method proposed by Grigorescu et al. [6,34] to evaluate the performance of these contour detectors. The method is reproduced here for completeness.

$$\mathbb{P} = \frac{card(E)}{card(E) + card(E_{FP}) + card(E_{FN})} \tag{19}$$

where $card(X)$ denotes the number of elements of set X;E,E_{FP},E_{FN} denote correctly detected contour pixels, false positives, false negatives, respectively.

For a better illustration, we also compute the fraction of false positives $\mathbb{F}_{FP}$ and the fraction of false negatives $\mathbb{F}_{FN}$. They are defined as fellows:

$$\mathbb{F}_{FP} = card(E_{FP})/card(E) \tag{20}$$

$$\mathbb{F}_{FN} = card(E_{FN})/card(E_{DO}) \tag{21}$$

where E_{DO} denotes the set of contour pixels of the desired output contour map, (see [6,34] for details). It is clear from the definitions that the nearer to 1 is the measure $\mathbb{P}$, the better is the result, whereas the nearer to 0 are the measures $\mathbb{F}_{FP}$ and $\mathbb{F}_{FN}$, the better is the result. Tables 1–3 list the fractions of false negatives, the fractions of false positives and the performance measures of examples shown in Figs. 7 and 8, respectively.

The performance measures show that our model has the better ability to detect contours in cluttered background,

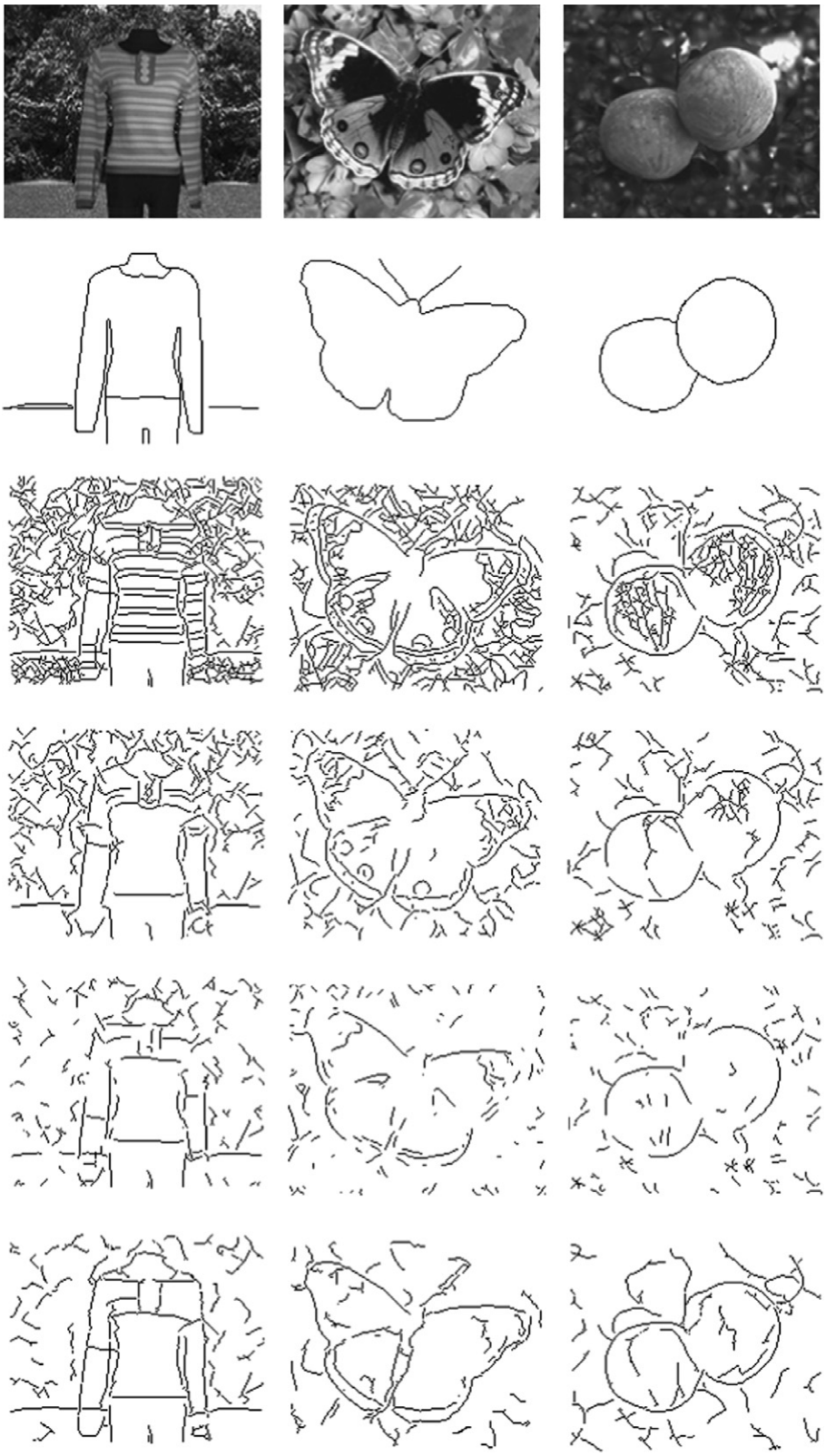

Fig. 8. The results of detecting contour with various operators. Panels from top to bottom correspond to input images (sized 150×180), desired outputs, the contours obtained with Gabor energy operator, the contours obtained with anisotropic inhibition operator, the contours obtained with isotropic inhibition operator, the contours obtained with our proposal. The left, middle and right panels (i.e. model, butterfly and orange) correspond to the three spatial frequencies $F = 0.2250$, 0.3375, 0.2250, respectively.

Table 1
The fractions of false negatives $\mathbb{F}_{FN}$

	Gabor energy	Anisotropic	Isotropic	Our proposal
Circle	0.05	0.48	0.63	0.06
Model	0.09	0.14	0.25	0.13
Butterfly	0.02	0.08	0.38	0.13
Orange	0.05	0.16	0.27	0.05

Table 2
The fractions of false positives $\mathbb{F}_{FP}$

	Gabor energy	Anisotropic	Isotropic	Our proposal
Circle	4.31	2.17	1.06	0.76
Model	4.69	2.30	1.34	1.21
Butterfly	7.05	3.47	2.51	2.18
Orange	6.93	4.37	2.82	2.80

Table 3
The performance measures $\mathbb{P}$

	Gabor energy	Anisotropic	Isotropic	Our proposal
Circle	0.19	0.24	0.27	0.55
Model	0.17	0.29	0.37	0.42
Butterfly	0.12	0.22	0.24	0.30
Orange	0.13	0.18	0.24	0.26

and at the same time, dramatically suppress surrounding textures.

4. Conclusions

Contour plays a key role in shape-based object recognition. Traditional edge detection algorithms do not distinguish between contours and edges, therefore the detected results contain plenty of unwanted elements. Grigorescu et al., have introduced the property of non-classical receptive field inhibition in primary visual cortex to contour detection. The proposal can reduce texture edges and retained isolated contours. However, when contours with coherent spatial configurations are embedded in the cluttered background, using only the inhibition mechanism makes difficult to obtain satisfactory results. In order to make up the deficiency of the method, we further introduce the enhancement mechanism in this paper. Our model makes full use of the configurational feature of smooth contours. Owing to collinear enhancement, smooth contours are not destructed by surround inhibition, while textures are suppressed to a large extent. Although the proposed model is as yet very primitive compared to the actual visual mechanisms, our results show that the approach is feasible to detect smooth contours from a cluttered or textured background that cannot be easily detected by others.

The present work may be improved further by adopting different local scales according to local features of an image, which can more accurately extract local edges and provide more integration information for local element grouping. Furthermore, iso-orientation suppression can be generalized to other homogeneity (such as color, frequency, contrast etc) suppression, which can pop-out conspicuous objects from uniform background. These are the work we plan to extend.

Acknowledgements

We thank the two anonymous reviewers for their comments and advice. This work was supported by the National Natural Science Foundation of China under Contract 60135020.

References

[1] J.F. Canny, A computational approach to edge detection, IEEE Trans. Pattern Anal. Mach. Intell. 8 (6) (1986) 679–698.
[2] R. Mehrotra, K.R. Namuduri, N. Ranganathan, Gabor filter-based edge detection, Pattern Recognit. 25 (12) (1992) 1479–1494.
[3] L.A. Iverson, S.W. Zucker, Logical/Linear operators for image curves, IEEE Trans. Pattern Anal. Mach. Intell. 17 (10) (1995) 982–996.
[4] M.H.F. Wilkinson, Optimizing edge detectors for robust automatic threshold selection: coping with edge curvature and noise, Graph. Models Image Process. 60 (4) (1998) 385–401.
[5] W.E. Higgins, C. Hsu, Edge detection using 2D local structure information, Pattern Recognit. 27 (2) (1994) 277–294.
[6] C. Grigorescu, N. Petkov, M.A. Westenberg, Contour detection based on nonclassical receptive field inhibition, IEEE Trans. Image Process. 12 (7) (2003) 729–739.
[7] G. Rizzolatti, R. Camarda, Inhibition of visual responses of single units in the cat visual area of the lateral suprasylvian gyrus (Clare-Bishop area) by the introduction of a second visual stimulus, Brain Res. 88 (2) (1975) 357–361.
[8] Y. Bonneh, D. Sagi, Effects of spatial configuration on contrast detection, Vis. Res. 38 (1998) 3541–3553.
[9] C. Blakemore, E.A. Tobin, Lateral inhibition between orientation detectors in the cat's visual cortex, Exp. Brain Res. 15 (1972) 439–440.
[10] A. Grinvald, E.E. Lieke, R.D. Frostig, R. Hildesheim, Cortical point-spread function and long range interactions revealed by real-time optical imaging of macaque monkey primary visual cortex, J. Neurosci. 14 (1994) 2545–2568.
[11] M.K. Kapadia, M. Ito, C.D. Gilbert, G. Westheimer, Improvement of visual sensitivity by changes in local context: parallel studies in human observers and in v1 of alert monkeys, Neuron 15 (1995) 843–856.
[12] U. Polat, A.M. Norcia, Neurophysiological evidence for contrast dependent long range facilitation and suppression in the human visual cortex, Vis. Res. 36 (1996) 2099–2109.
[13] J.B. Levitt, J.S. Lund, Contrast dependence of contextual effects in primate visual cortex, Nature 387 (1997) 73–76.
[14] J.J. Knierim, D.C. van Essen, Neuronal responses to static texture patterns in area V1 of the alert macaque monkeys, J. Neurophysiol. 67 (1992) 961–980.
[15] M.K. Kapadia, M. Ito, C.D. Gilbert, G. Westheimer, Improvement in visual sensitivity by changes in local context: parallel studies in human observers and in V1 of alert monkeys, Neuron 15 (1995) 843–856.
[16] Z. Li, Visual segmentation by contextual influences via intracortical interactions in primary visual cortex, Comput. Neural Syst. 10 (1999) 187–212.
[17] U. Polat, K. Mizobe, M.W. Pettet, T. Kasamatsu, A.M. Norcia, Collinear stimuli regulate visual responses depending on cell's contrast threshold, Nature 391 (1998) 580–584.

[18] Z. Li, A saliency map in primary visual cortex, Trends Cogn. Sci. 6 (1) (2002) 9–16.
[19] Q. Tang, N. Sang, T. Zhang, A Neural Network Model for Extraction of Salient Contours. International Symposium on Neural Networks (ISNN'05), Springer-Verlag, Berlin Heidelberg, 2005, 316–320.
[20] J. Xing, D.J. Heeger, Measurement and modeling of center-surround suppression and enhancement, Vis. Res. 41 (2001) 571–583.
[21] J.I. Nelson, B.J. Frost, Orientation-selective inhibition from beyond the classic visual receptive field, Brain Res. 139 (1978) 359–365.
[22] R.L. de Valois, E.W. Yund, N. Hepler, The orientation and direction selectivity of cells in macaque visual cortex, Vis. Res. 22 (1982) 531–544.
[23] J.A. Movshon, I.D. Thompson, D.J. Tolhurst, Spatial summation in the receptive fields of simple cells in the cat's striate cortex, J. Physiol. 283 (1978) 53–77.
[24] J.G. Daugman, Uncertainty relation for resolution in space, spatial frequency, and orientation optimized by two-dimensional visual cortical filters, J. Opt. Soc Am. A. 2 (7) (1985) 160–1169.
[25] J.J. Koenderink, A.J. van Doom, Receptive field families, Biol. Cybern. 63 (1990) 291–298.
[26] M. Porat, Y.Y. Zeevi, The generalized Gabor scheme of image representation in biological and machine vision, IEEE Trans. Pattern Anal. Mach. Intell. 10 (4) (1988) 452–468.
[27] A.K. Jain, F. Farrokhnia, Unsupervised texture segmentation using Gabor filters, Pattern Recognit. 24 (12) (1991) 1167–1186.
[28] M.C. Morrone, D.C. Burr, Feature detection in human vision: a phase-dependent energy model, Proc. R. Soc. Lond. [Biol.] 235 (1988) 221–245.
[29] W. Chan, G. Coghill, Text analysis using local energy, Pattern Recognit. 34 (2001) 2523–2532.
[30] S. Marcelja, Mathematical description of the responses of simple cortical cells, J. Opt. Soc. Am. 70 (1980) 129–130.
[31] D.A. Pollen, S.F. Ronner, Spatial computation performed by simple and complex cells in the visual cortex of the cat, Vis. Res. 22 (1982) 101–118.
[32] F. Heitger, L. Rosenthaler, R. von der Heydt, E. Peterhans, O. Kübler, Simulation of neuronal contour mechanisms: from simple to end-stopped cells, Vis. Res. 32 (1992) 963–981.
[33] E.R. Hancock, J. Kittler, Adaptive estimation of hysteresis thresholds, Proc. IEEE Conf. Comput. Vis. Pattern Recognit. (1991) 196–201.
[34] C. Grigorescu, N. Petkov, M.A. Westenberg, Contour and boundary detection improved by surround suppression of texture edges, Image Vis. Comput. 22 (8) (2004) 609–622.